Journal of Physics: Conference Series **712** (2016) 012106 doi:10.1088/1742-6596/712/1/012106

Structure analyses of Cu nanoclusters in the soft magnetic $Fe_{85.2}Si_1B_9P_4Cu_{0.8}$ alloy by XAFS and fcc cluster model

M Matsuura[1], M Nishijima[1], K Konno[2], H Ofuchi[3], K Takenaka[1], A Makino[1]

[1] Research and Development Center for Ultra High Efficiency Nano-crystalline Soft Magnetic Material, Institute for Materials Research, Tohoku University, Sendai 980-8577, Japan

[2] Sendai National College of Technology, Medeshima, Natori, Miyagi 981-1239, Japan

[3] Industrial Application Division, Japan Synchrotron Radiation Research Institute (JASRI), Kouto, Sayo, Hyogo 679-5198, Japan

E-mail:m_matsuura@imr.tohoku.ac.jp

Abstract. Size of the clusters and structure details of fcc Cu clusters in nanocrystalline soft magnetic alloy of $Fe_{85-86}Si_{1-2}B_8P_4Cu_1$ (NANOMET) are investigated. A linear combination fitting of XAFS data indicates that about 30% of Cu atoms are partitioned in the fcc clusters and the rest in the amorphous matrix. EXAFS of the fcc Cu nanocluster embedded in amorphous matrix is calculated on the basis of a simple fcc structure model using FEFF9. Surface effect of the nanoclusters is considered by counting a fraction of the nearest neighbour atoms in amorphous matrix. Good agreement with the experimental result is obtained for the fcc nanocluster with 9 coordination shells which consists of total 177 atoms within 1.5 nm in a diameter.

1. Introduction

Nanocrystalline soft magnetic alloys have been attracted much attention because of their high saturation magnetic flux density (B_s), low coercivity (H_c) and low magnetic core loss (W). Those soft magnets, however, exhibit relatively low B_s compared with a conventional silicon steel (Fe-3.5wt. % Si) with 2 T. Recently Makino et al. have developed a new Fe-based alloy of $Fe_{85-86}Si_{1-2}B_8P_4Cu_1$ (NANOMET) which exhibits high B_s (1.82~1.85 T) together with low H_c (2.6~5.8 A/m) and considerably low W [1-2]. These superior soft magnetic properties of NANOMET originate from the precipitated α-Fe nanocrystallites embedded in a residual amorphous matrix. NANOMET contains a small amount of Cu, ~1 at%, which effectively reduces the grain size of the precipitated α-Fe crystallites to a nanometer scale [3]. It is not, however, well understood about the role of Cu in the nanocrystallization of precipitated α-Fe crystallites. Because of a dilute content of Cu (<1.0 at%), conventional structural analyses, XRD and TEM, are inappropriate, whereas XAFS, especially fluorescence XAFS, is an advantageous tool for studying the local structure of a dilute element. In the previous work the authors observed the local structure changes around Cu in NANOMET during nanocrystallization by XAFS [4-5]. These XAFS results and TEM observations [6] conform that fcc Cu clusters are formed prior to the α-Fe precipitation like as the case of FINEMET [7-9]. But unlike

FINEMET fcc Cu clusters in NANOMET transform into bcc structure in the early stage of α-Fe precipitation. In this paper we calculated EXAFS of the fcc Cu nanoclusters based on a simple fcc structure model and estimated the size of the cluster.

2. EXAFS calculation of the fcc Cu nanoclusters embedded in amorphous matrix

Cu atoms are distributed both in fcc Cu clusters and amorphous matrix. So at first, the distribution fractions of Cu in the two phases are evaluated from the experimental data. Secondly, EXAFS functions $\chi(k)_{fcc\ cluster}$ of the model fcc Cu clusters are calculated using FEFF9. Thirdly, fraction of the nearest neighbour atoms outside clusters x is calculated. Contribution of Cu in amorphous matrix surrounding fcc clusters is estimated from the fraction x and $\chi(k)_{amor}$ deduced from the experimental data.

2.1. Fraction of Cu partitioned into fcc Cu clusters.

Figure 1 shows results of the Cu K-edge EXAFS in terms of radial structure function (RSF) of the as-quenched, annealed at 340°C and 700°C for $Fe_{85.2}Si_1B_9P_4Cu_{0.8}$ alloy together with that of a Cu foil. XAFS measurements were carried out at BL14B2 in SPring-8 by a fluorescence mode using 19-elements SSD at 10-20K. Experimental details were described in the previous works [4-5]. The RSF of the as-quenched ribbon shows a typical of amorphous structure and those of the annealed at 340°C and 700°C show an fcc structure. In the previous papers, authors proved that Cu atoms form fcc clusters prior to α-Fe precipitation and they segregate above the second crystallization temperature (T_{x2}=571°C) [4-5]. Here we try to analyze the fcc Cu clusters formed during nanocrystallization of $Fe_{85.2}Si_1B_9P_4Cu_{0.8}$ alloy. Cu atoms in the sample annealed at 340°C are partitioned both into the fcc Cu clusters and amorphous matrix. The EXAFS function of the annealed at 340°C, $\chi(k)_{340℃}$, can be described as

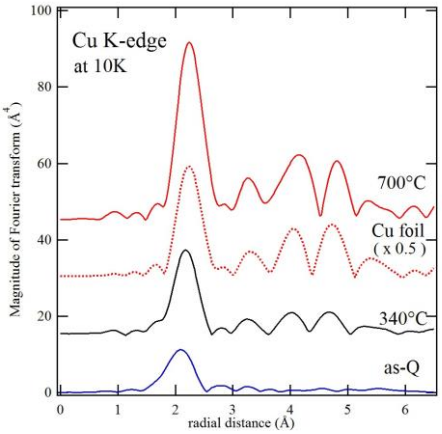

Figure 1. Radial structure functions of the Cu K-edge for $Fe_{85.2}Si_1B_9P_4Cu_{0.8}$ alloy: as-quenched, annealed at 340°C and 700°C together with a Cu foil.

$$\chi(k)_{340℃} = \alpha \cdot \chi(k)_{fcc\ cluster} + (1-\alpha) \cdot \chi(k)_{amor.} \quad (1)$$

, where α is a fraction of Cu atoms included in the fcc clusters, (1-α) a fraction of those in the amorphous matrix, $\chi(k)_{fcc\ cluster}$ an EXAFS function of the fcc Cu clusters and $\chi(k)_{amor.}$ that of the amorphous matrix. α is estimated by fitting the $\chi(k)_{340℃}$ to a linear combination of these data of $\chi(k)_{700℃}$ and $\chi(k)_{as\text{-}quench}$ which are considered to correspond to $\chi(k)_{fcc\ cluster}$ and $\chi(k)_{amor.}$, respectively in equation (1). The estimated value of α is 0.29, i.e. around 30% of Cu atoms contribute to form fcc clusters and the rest are in the amorphous matrix. We thus can evaluate $\chi(k)_{fcc\ cluster}$ in equation (1) to which the calculation is compared.

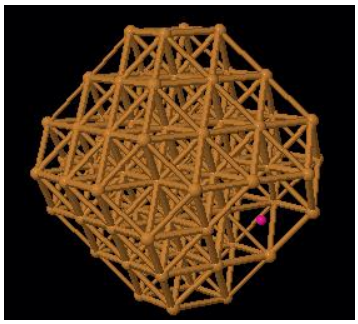

Figure 2. Scattering atoms within the clusters when an absorbing atom (shown as pink color) locates in the third coordination shell of the *5-th* cluster.

2.2. Structure model of an fcc Cu nanocluster.

The fcc Cu clusters in NANOMET are assumed to consist exclusively of Cu atoms, i.e. pure Cu, and a size distribution of the fcc clusters is neglected. Coordinates, (x,y,z)'s, are assigned to all

atoms in the cluster of which center is (0,0,0). We call the "*n-th* cluster" which has the outermost coordination shell of *n*. Figure 2 shows all the scattering atoms of the clusters when an absorbing atom (colored with pink) locates in the third coordination shell of the *5-th* cluster. When the specific coordination shell *j* of the *n-th* cluster consists of N_j atoms, the EXAFS functions, $\chi(k)_{n,j}$, of those atoms in the *j*-th shell are same because they have same symmetry. The $\chi(k)_{n,j}$'s are calculated for all coordinate shell, j=1, 2, , ,*n*, supposing an isolated fcc Cu cluster, i.e. nothing is surrounded around the cluster, using ab initio calculation code of FEFF9 [10]. Finally the EXAFS function of the isolated *n-th* cluster $\chi(k)_{n,i}$, is calculated by averaging over all atoms $N(=1+\sum_{j=1}^{n} N_j)$ in the cluster using equation (1):

$$\chi(\mathrm{k})_{n,i} = \frac{\sum_{j=1}^{n} N_j \chi(k)_{n,j}}{N} \quad (1)$$

2.3. Contribution of the amorphous matrix: surface effects of the nanocluster.

Because the Cu clusters in NANOMET are embedded in the amorphous matrix, photo electrons emitted from atoms close to the surface of the cluster are scattered by amorphous matrix. Contribution from amorphous matrix to $\chi(k)$ is not easy to evaluate exactly but as indicated in Figure 1 the RSF of the as-quenched one has only one small peak of the nearest neighbor shell. When an absorbing atom near the surface has *p* nearest neighbors within the cluster, then we assume that the nearest neighbor atoms in the amorphous matrix are *12-p* atoms. A fraction of the nearest neighbor atoms, *x*, outside the cluster to the total nearest neighbor atoms, i.e. $N_{nn}(=12\times N)$, is evaluated by following equation:

$$x = \frac{\sum_{j=0}^{n} N_{j,o}}{N_{nn}} \quad (2)$$

, where $N_{j,o}$ is number of the nearest neighbor atoms in the amorphous matrix around an atom in the *j-th* coordinate shell. EXAFS of the *n-th* cluster $\chi(k)_n$ can be described as:

$$\chi(k)_n = (1-x)\chi(k)_{n,i} + x\cdot\chi(k)_{n,o} \quad (3)$$

, where $\chi(k)_{n,o}$ is $\chi(k)$ contributed from atoms outside the cluster which is substituted by $\chi(k)_{as-quench}$.

2.4. Calculated results of EXAFS for the fcc Cu nanocluster.

In the calculation a coordination shell around a center of the cluster is changed from *n*=1 to 12, which corresponds to 0.512 nm to 1.77 nm in diameter of the clusters in which *N*=13 to 249 atoms are included. In the calculation an interatomic distance is 0.250 nm, which leads to fit the first peak of the RSF to the experimental data. Figure 3 shows calculated results of the RSF of the fcc Cu clusters with a different coordination shell (*n*=3, 9 and 12), together with the $\chi(k)_{fcc\ cluster}$ reduced from the experimental data. Cluster diameters are 0.88, 1.53, 1.77 nm for *n*=3, 9, 12. As a matter of course, surface effect of a cluster increases with decrease in a cluster size; the *3rd*-cluster, has the lowest RSF peaks and besides they attenuate rapidly with increase in a radial distance and the RSF curve of the *12-th* cluster exhibits the most similar features to that of a Cu foil among other cases. Figure 3 shows that the result of the *n*=9 exhibits the best agreement with that of the $\chi(k)_{fcc\ cluster}$. Below and above *n*=9 the agreement becomes poorer than that of *n*=9. From these results it can be said that about 30% of Cu atoms in $Fe_{85.2}Si_1B_9P_4Cu_{0.8}$ alloy are partitioned in the fcc

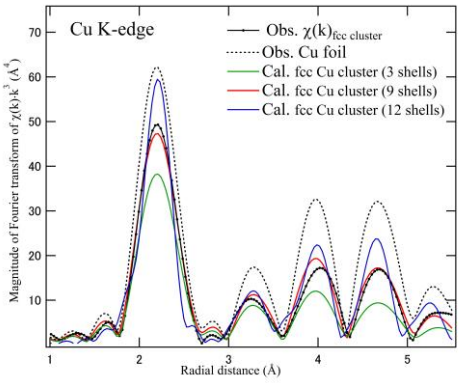

Figure 3. Calculated RSFs of the fcc Cu clusters with different coordination shells: n=3, 9, and 12, together with the experimental results of the $\chi(k)_{fcc\ cluster}$ and a Cu foil.

Cu clusters and size of the fcc nanocluster is about 1.8 nm and 249 atoms are included in it. The value of 1.8 nm in size of the cluster agrees with a recent TEM observation [6]

3. Discussion

The Cu K-edge EXAFS of $Fe_{85.2}Si_1B_9P_4Cu_{0.8}$ alloy shows that local structure around Cu changes in a sequence of "amorphous→fcc→bcc→fcc" in the cause of nanocrystallization [4-5]. Here, we focus our attention to the structure of the fcc clusters formed prior to the α-Fe precipitation. A fraction of Cu atoms α which form fcc clusters embedded in amorphous matrix is determined by a liner combination fitting (LCF). In the LCF procedures data of the $\chi(k)_{700℃}$ is applied rather than that of a Cu foil because the segregated Cu crystals are more similar to the fcc Cu clusters rather than a Cu foil: concentration and surface effects. Interatomic distance which can fit to the experiments in the calculation is 0.250 nm. This value is a little bit shorter than that of a Cu foil, 0.2556 nm. Probably it stems from that in the present calculation the nanoclusters are assumed to consist only from Cu but actually some Fe atoms are also included in it. A whole future of the EXAFS function of the present fcc cluster alters little if some fraction of Cu atoms are replaced by Fe atoms. Although the present fcc cluster model can fit the experimental EXAFS result, it cannot explain how fcc Cu clusters contribute nanocrystallization of precipitated α-Fe crystallites. Previous XAFS work [4] indicates that before the onset of α-Fe precipitation (T_{x1}=432°C), fcc structure of Cu clusters transforms into bcc and TEM observation shows that nanometer size Cu rich particles are observed mostly at around peripheral of α-Fe nanocrystallites [6]. From these facts α-Fe precipitation occurs preferentially nearby fcc Cu clusters and surface energy at interfaces between the fcc Cu clusters and bcc Fe crystals may cause to transform structure of Cu clusters from fcc to bcc. The Cu K-edge EXAFS data indicates that the sample annealed at 340°C shows fcc structure and bcc at 380°C, and it shows mixture of fcc and bcc at 365°C. It is necessary to examine whether this structure model of the fcc clusters can explain such a structure transformation, which will be presented somewhere else in near future.

4. Acknowledgements

The synchrotron radiation experiments were performed at the BL14B2 of SPring-8 with the approval of the Japan Synchrotron Radiation Research Institute (JASRI) (Proposal Nos. 2013A1641, 2013B1715, 2014A1705, 2014B1794 and 2015A1850). This work was financially supported by Ministry of Education, Culture, Sports, Science and Technology (MEXT), Japan under "Tohoku Innovative Materials Technology Initiatives for Reconstruction" project, "Ultra-low Core Loss Magnetic Material Technology Area."

References

[1] Makino A, Kubota T, Yubuta K, Inoue A, Urata A, Matsumoto K and Yoshida S 2011 *J. Appl. Phys.* **109** 07A302-1.
[2] Makino A, Men H, Kubota T, Yubuta K, and Inoue A 2009 *Mater. Trans.* **50** 204.
[3] Cui L, Men H, Makino A, Kubota T, Yubuta K, Qi M and Inoue A 2009 *Mater. Trans.* **50** 2515.
[4] Nishijima M, Matsuura M, Takenaka K, Takeuchi A, Ofuchi H and Makino A 2014 *AIP Adv.* **4** 057129.
[5] Matsuura M, Nishijima M, Takenaka K, Takeuchi A., Ofuchi H and Makino A 2015 *J. Appl. Phys.* **117** 17A324.
[6] Nishijima M, Matsuura M, Zhang Y and A Makino 2015 *Phil. Mag. Let.* 2015 **95** 277.
[7] Yoshizawa Y, Oguma S and Yamauchi K 1988 *J. Appl. Phys.* **64** 6044.
[8] Kim S H, Matsuura M, Sakurai M and Suzuki K 1993 *Jpn. J. Appl. Phys*. Part 1 **32**(Suppl. 32-2) 676.
[9] Ayers J D, Harris V G, Sprague J A, Elam W T and Jones H N 1998 *Acta Mater*. **46** 1861.
[10] Rehr J J, Kas J J,Vila F D, Prange M P and Jorissen K 2010 *Phys. Chem. Chem. Phys*. **12** 5503-5513.